INTERNATIONAL JOURNAL OF HYDROGEN ENERGY XXX (2017) 1–10

Available online at www.sciencedirect.com

ScienceDirect

journal homepage: www.elsevier.com/locate/he

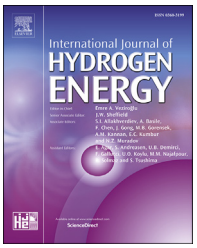

# N-doped porous carbon from *Sargassum* spp. as metal-free electrocatalysts for oxygen reduction reaction in alkaline media

*B. Escobar* [a,*], *K.Y. Pérez-Salcedo* [b], *I.L. Alonso-Lemus* [c], *D. Pacheco* [b], *Romeli Barbosa* [d]

[a] CONACYT – Centro de Investigación Científica de Yucatán, Carretera Sierra Papacal – Chuburná Puerto, Km 5. Sierra Papacal, Mérida, C.P 97302, Yucatán, Mexico

[b] Centro de Investigación Científica de Yucatán, Carretera Sierra Papacal – Chuburná Puerto, Km 5. Sierra Papacal, Mérida, C.P 97302, Yucatán, Mexico

[c] CONACYT – Centro de Investigación y Estudios Avanzados Del IPN Unidad Saltillo, Av. Industria Metalúrgica, Parque Industrial Saltillo-Ramos Arizpe, C.P 25900, Ramos Arizpe, Coahuila, Mexico

[d] Universidad de Quintana Roo, Boulevard Bahía S/n, Chetumal, C.P 77019, Quintana Roo, Mexico

ARTICLE INFO

*Article history:*
Received 16 March 2017
Received in revised form
11 May 2017
Accepted 30 June 2017
Available online xxx

*Keywords:*
Self-doped porous carbon
*Sargassum* spp.
Oxygen reduction reaction
Pyrolysis

ABSTRACT

The use of *Sargassum* spp. as raw material for the synthesis of metal-free electrocatalyst was studied. Besides, it offers an interesting alternative to low cost commercial activated carbons with applications in generation and storage energy. In this work, physicochemical and electrochemical properties of pyrolyzed, activated and doped carbons synthesized from this abundant seaweed have been studied. Graphitic carbon formation after pyrolysis was confirmed by Raman spectroscopy. SBET increase after activation and doping treatment was corroborated by BET. Electrochemical analyses demonstrated that the SAC sample exhibits the highest ORR activity and showed a current density (4.78 mA $cm^{-2}$) close to commercial 20 wt% Pt/C (5.6 mA $cm^{-2}$) evaluated at the same conditions. Moreover, SDO sample shows the better onset potential (0.852 V vs. RHE), which is in accordance with the content of N-pyridinic bonds on its surface. These results suggest that SDO and SAC biocarbons from *Sargassum* spp. are a promising cathode material for fuel cells.



## Introduction

Oceans have approximately half of the global biodiversity, so they can be considered as a potential source of resources. Therefore, seaweeds are renewable and abundant source of carbon and other heteroatoms. Thus, seaweeds annual production has been calculated about 2.6 million tons of red algae and 16 million tons of brown algae [1]. In the last years, extensive pelagic *Sargassum* spp. inundation covered tourist beaches in Caribbean, Gulf of Mexico, West African, and Brazilian by more than a meter of seaweed [2]. These massive beaching events began recording strongly since 2011 [3]. Economic impacts on the tourist industry of the Mexican Caribbean suggest that it is urgent to generate alternatives for the

* *Corresponding author.*
E-mail addresses: bem08@hotmail.com, beatriz.escobar@cicy.mx (B. Escobar).

http://dx.doi.org/10.1016/j.ijhydene.2017.06.240

use of this abundant waste from the sea. Thus, *Sargassum* spp. can be considerate a prolific source of carbon and other compounds (N ≈ 2–6%) [4]. Therefore, its study as raw material in the field of energy conversion and storage is interesting and promising.

Pyrolysis is the most common process for converting biomass into carbon. This process does not require advanced technology, and often is performed at temperatures between 400 and 1000 °C in a controlled atmosphere ($N_2$ or Ar). In this way, pyrolysis process is a very feasible option to obtain biocarbons from abundant biomass wastes as *Sargassum* spp., which is currently deposited in large quantities on the beaches of Cancun Quintana Roo Mexico, and has no commercial use. However, biocarbons obtained from pyrolysis have low porosity and low specific surface area; therefore, it is necessary an additional treatment of activation by chemical or physical methods to increase the potential use of pyrolytic carbons [5].

Carbon is widely used as support for electrochemical energy conversion in fuel cells and batteries. Several types of carbons have been studied as electrocatalyst support of Pt alloys or non-precious transition metal to reduce or replace Pt [6]. Recently, novel nitrogen-doped carbons (N-carbons) have emerged as the most promising metal-free electrocatalyst for cathodes of alkaline fuel cells. It has been reported that N-carbons have high performance for the ORR in alkaline and acid media. These electrocatalyst are an attractive alternative due at their low cost, high stability and environmental friendly [7]. Incorporation of nitrogen into carbon lattice modified the properties of carbon support providing high electrical conductivity and excellent capacitive performance. Fermi level is shifted to the valence band with N incorporation, thereby facilitating the electron transfer [8]. Nitrogen-doped carbons has been synthetized in situ during the carbon synthesis using N precursors as dicarboxylic acids [9], citric acid [10], amino acids [11] or hydrazine. Chemical deposition of N and C precursors as melanin and amino sugars is other explored method. The pyrolysis temperature allows controlling the graphitization degree, surface area and the nitrogen species formed [12].

N-carbons are the most reported metal-free electrocatalyst for the ORR. However, doped carbons with boron, sulfur and phosphorus for energy applications has been less explored [13]. Recently, the use of biomass as C and heteroatoms source has been proposed for the synthesis of metal-free electrocatalyst and catalyst support. Chicken feathers [14], urine [15], yeast cells [16], industrial waste from olive oil [17], soybeans [18], zinc chloride promote soybeans [19], and 'okara' a byproduct from tofu and soy milk production, which is commonly used as feed for livestock or as natural nitrogen fertilizer [20] have been explored as raw material of metal-free electrocatalyst with promising electrochemical performance. Huang et al. 2016, reported the use of *Malachium aquaticum*, a plant from China as raw material for obtaining efficient N-doped electrocatalyst for ORR. In their work, different pyrolysis temperatures were evaluated (700 °C, 800 °C and 900 °C). The sample pyrolyzed at 900 °C shows the best ORR performance due to better active sites and superior electrical conductivity regarding to the samples synthesized at lower temperatures [21]. Also, the synthesis of N-doped porous carbon aerogels using soy protein as C and N precursor has been reported [22]. In addition, *Enteromorpha algae* is a green macroalgae that can be accumulated in massive quantities, this phenomenon is named as a "green tide" which can damage the marine ecosystem. This abundantly available C and N precursor was used to obtain a high-value-added porous carbon structure, which was activated using KOH and nitrogen atmosphere at 800 °C obtaining high specific surface area.

The commercial costs of different carbon structures used in electrocatalyst field are very varied, for instance, the price (USD/gram) of Vulcan XC-72 is 1 USD/g and Pt/Vulcan on rises to 69 USD/g [23]; activated charcoal (Sigma Aldrich), 1.8 USD/g; MWCNT, 15 USD/g. In this work, we use *Sargassum* spp. as raw material in the synthesis of N-doped porous carbon for metal-free electrocatalysts for ORR in alkaline media. Activation and doping was performed with KOH and hydrazine, respectively. The aim of this work, in a first stage is to study the physicochemical and electrochemical properties of N-doped carbons from *Sargassum* spp. and their performance as a potential metal-free electrocatalyst for the ORR in alkaline fuel cells.

## Experimental method

### *Metal-free electrocatalyst synthesis*

*Sargassum* spp. was collected from the Caribbean beach, in the Cancun and Playa del Carmen coasts, in Quintana Roo, Mexico. Once collected was washed with distilled water and ethanol to remove clay sands, dusts, sediments, shells and pebbles. After, it was filtered and pulverized until an average particle size around of 75 μm. The dried seaweed (RS sample) was pyrolyzed in a tubular horizontal furnace at 700 °C during 90 min with a heating rate of 10 °C $min^{-1}$ under a nitrogen flow of 50 mL $min^{-1}$ (SPY sample). SPY was subjected at two treatments previously reported [24]. Doping treatment was carried out dispersing 1 g of SPY in 30 mL of hydrazine (Sigma-Aldrich, 50–60%). The dispersed solution was placed in a sealed steel autoclave for the solvothermal treatment, this was carried out at 180 °C during 24 h. Then, the powder was recovered by filtration, washed with distilled water and dried at 80 °C overnight (SDO sample). Otherwise, the activation treatment was carried out mixing SPY and KOH (Sigma-Aldrich, 90%) at a mass ratio 1:2; then was heated at 600 °C during 90 min with increases of 8 °C $min^{-1}$ in $N_2$ atmosphere. The sample was washed with 1 M HCl solution (Sigma-Aldrich, 37%) to remove the residual alkali. Finally, the powder was dried at 80 °C overnight (SAC sample).

### *Physical-chemical characterization*

Nitrogen adsorption-desorption analysis was carried out in a Quantachrome Nova 2200e. The Brunauer–Emmett–Teller (BET) equation was employed to calculate the surface area of the metal-free electrocatalysts. Prior to analysis the samples were degassed at 200 °C during 8 h. Raman spectra was recorded in a Thermoscientific DRX Raman with a HeNe gas laser (λ = 633 nm). Elemental analysis (C, H, N and S) was carried out using a Thermoscientific Elemental Analyzer Flash

Please cite this article in press as: Escobar B, et al., N-doped porous carbon from *Sargassum* spp. as metal-free electrocatalysts for oxygen reduction reaction in alkaline media, International Journal of Hydrogen Energy (2017), http://dx.doi.org/10.1016/j.ijhydene.2017.06.240

2000. All the measurements were repeated tree times and the value reported is the average value. Chemical surfaces composition of RS and the metal-free electrocatalysts were analyzed by X-ray photoelectron spectroscopy (XPS) using a Thermoscientific K-Alpha equipped with an Al Kα X-ray source. Functional groups on the carbon surface were determined by Fourier transform infrared spectroscopy (FTIR) with Bruker FT-IR Tensor II. This analysis was carried out with the ATR (Attenuated Total Reflection) accessory. Morphological characterization was also carried out by Scanning Electron Microscopy with a Philips XL30E SEM microscopy. The thermogravimetric analysis (TGA) of all samples was carried out using a Perkin Elmer TGA 800. TG curve was obtained under a nitrogen atmosphere with a flow rate of 10 mL $min^{-1}$, heating rate of 10 °C $min^{-1}$ from 25 to 700 °C with a sample mass of 10 mg in a platinum pan. The mass loss rate in the derivative form (DTG) was also calculated.

### *Electrochemical characterization*

Electrochemical experiments were performed with a Biologic VSP300 potentiostat in a conventional three-electrode test cell at room temperature. An Ag/AgCl (KCl saturated) was used as reference electrode and a platinum wire as counter electrode. Working electrode was a 5 mm diameter glassy carbon embedded in Teflon. Before measurements working electrode was polish with 0.05 μm' alumina slurries to a mirror finish. The homogeneous catalyst ink was made by mixture of 20 mg catalyst, 60 μL Nafion ionomer solution and 1 mL ethanol. For cyclic voltammetry (CV), window potential was chosen from 1.2 V to 0.05 V vs. RHE and 20 $mVs^{-1}$ scan rates for 3 cycles, also before measurements an activation treatment was done at same potential window at 50 $mVs^{-1}$ scan rate for 40 cycles. The 0.5 M KOH electrolyte was saturated with nitrogen gas. ORR was performed using the rotary disc electrode (RDE) technique at 1.2 to 0.05 V vs. RHE in $O_2$ saturated electrolyte for 25 min (5 $mVs^{-1}$) at 200, 400, 800, 1200, 1600 and 2000 RPM rotation rates.

## Results and discussions

### *Thermogravimetric analysis*

TGA analysis revealed the changes occurred during *Sargassum* spp. pyrolysis treatment, providing useful information about the reactions involved in this process. *Sargassum* spp. pyrolysis can be divided into four stages. Fig. 1 shows mass TG and derivate mass DTG curves of RS sample. Stage I occurs between 50 and 150 °C, in which evaporation of water and some light volatiles of biomass takes place. Stage II happens at 150–250 °C where the decomposition of some volatile components were progressively released, resulting in a slightly weight loss and the formation of the main pyrolytic products. Also, polymerization and vitrification transformation process would take place [25]. The pyrolysis mainly happened in the stage III between 250 and 550 °C, this stage is known as devolatilization stage and the process corresponds to lost mass of the majority organic compounds of *Sargassum* spp. associated with carboxylic acid, phenolic species, methane and $CO_2$ [26]. Carbonaceous matter as solid residual in Stage IV (temperatures above 550 °C) indicates that the sample is mainly composed by coke and ash. The sample at 700 °C shows a TG curve was nearly flat, then, this temperature is appropriate for the *Sargassum* spp. pyrolysis treatment. Approximately 40 wt% of the initial material remained after pyrolysis treatment, which indicates high yields for this process using *Sargassum* spp. Table 1 summarizes the most important pyrolytic features of RS sample; these parameters are calculated from the DTG profile [27].

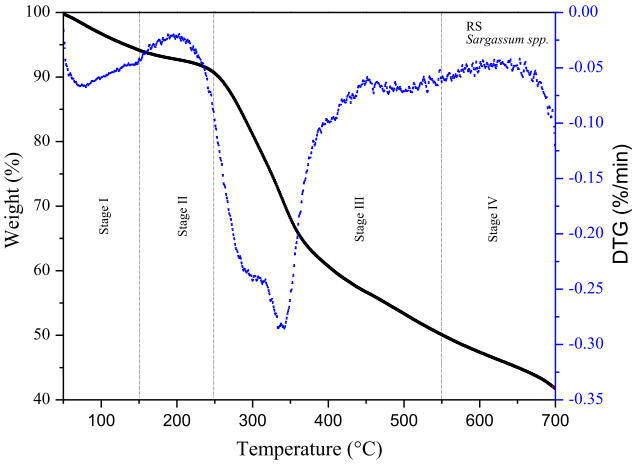


**Fig. 1 – TGA and DTG curves of *Sargassum* spp. (RS) in nitrogen atmosphere.**

### *Morphology*

Morphological features were observed by SEM to understand the structural changes occurring to RS sample after pyrolysis, activation and doping treatments. Fig. 2a–d shows the micrographs of a) RS, b) SPY, c) SDO and d) SAC samples. Fig. 2a) shows a typical micrograph of *Sargassum* spp. This material has a roughness surface of square macropores with uniform distribution. After pyrolysis treatment, SPY sample (Fig. 2b) shows an irregular and aggregated structure, where some of the pores might have been blocked by deposition of carbonaceous materials [13] reducing the BET area obtained for RS (Table 2). Considerable differences were observed after doping and activation treatments. SDO sample (Fig. 2c) shows very small aggregates over the carbon surface generated by solvothermal treatment. The small aggregates have influence in the increment of BET area for this sample. Finally, upon

**Table 1 – TGA-TDG pyrolysis analyses of raw *Sargassum* spp. (RS).**

| Temperature (°C) | 1st Shoulder | Peak | 2nd Shoulder | Peak |
|---|---|---|---|---|
| $T_{do}$ | 150 | | | |
| $T_{po}$ | – | 200 | 360 | 450 |
| $T_{pf}$ | – | 400 | 400 | 580 |
| $T_p$ | – | 310 | | 580 |

*$T_{do}$: Initial decomposition temperature; $T_{po}$: Initial peak temperature; $T_{pf}$: Final peak temperature; $T_p$: Peak temperature.

Please cite this article in press as: Escobar B, et al., N-doped porous carbon from *Sargassum* spp. as metal-free electrocatalysts for oxygen reduction reaction in alkaline media, International Journal of Hydrogen Energy (2017), http://dx.doi.org/10.1016/j.ijhydene.2017.06.240

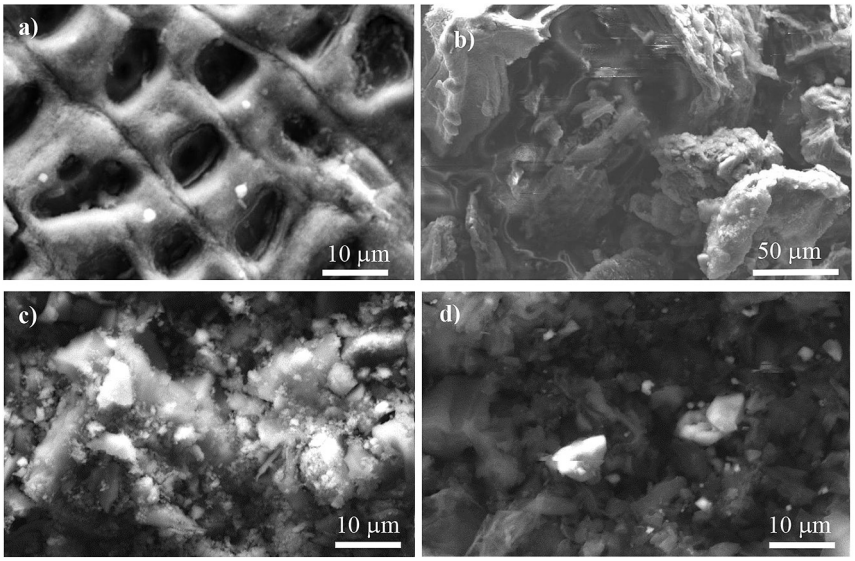


**Fig. 2 – SEM micrographs of a) RS, b) SPY, c) SDO and d) SAC materials.**

activation of SYP material, the BET surface area increase may be for the formation of micro-mesoporosity caused by the alkali. The surface morphology of SAC sample is irregular and roughness (Fig. 2d).

### *BET-analysis*

Textural properties of RS and N-doped electrocatalysts were determined by nitrogen adsorption/desorption analysis, the isotherms obtained are showed in Fig. 3. The specific surface area (SBET) was calculated using the BET equation. RS sample have a SBET of 34.42 $m^2 g^{-1}$. Moreover, the SBET after pyrolysis decrease significantly until 3.86 $m^2 g^{-1}$. The results reveal that the volatile compounds released during pyrolysis destroy the uniform surface of RS sample, decreasing the SBET in almost 10 times for SYP sample. These results are comparable with the reported by Lopez-Gonzalez [28], where after the pyrolysis of three types of microalgae between 300 and 600 °C found SBET from 2.0 to 3.2 $m^2 g^{-1}$. Furthermore, the SBET reduction is associated to the filling or blockage of micropores by high contents of ash, impeding the access of adsorbate gas, resulting in the production of low SBET carbons [29]. In the case of SDO sample, solvothermal treatment modified the surface generating small aggregates that increase the SBET. physical activation tends to enhance the development of the porous structure which has the highest value of 133.87 $m^2 g^{-1}$. Moreover, SAC sample has a SBET of 33 $m^2 g^{-1}$. This result indicates that the activation treatment is effective to promote the pores formation increasing the SBET with respect to the sample SYP. Table 2 summarized the textural properties as SBET, pore diameter and pore volume calculated from absorption/desorption analysis.

Pore diameter values of N-doped carbons indicate the existence of micropores and/or mesopores produced by the generation and release of gases during the cracking process of the organic species. Otherwise, SYP sample with diameter pore of 2.503 nm had an increase in this value respect to RS sample (from 2.503 to 4.288 nm). For the SDO sample the smallest pore diameter was observed, this can be attributed to the interstices formed between the small aggregates that were observed by SEM (≈1.902 nm). The pore diameter average decrease in SAC after activation while pore volume after activation remains very similar to RS sample.

**Table 2 – Textural properties of RS and N-doped porous carbon synthetized from *Sargassum* spp.**

| Samples | Pore diameter average (nm) | $S_{BET}$ ($m^2 g^{-1}$) | Pore volume ($cm^3$) |
|---|---|---|---|
| RS | 2.503 | 34.426 | 0.043 |
| SPY | 4.288 | 3.864 | 0.008 |
| SDO | 1.940 | 133.871 | 0.129 |
| SAC | 3.010 | 33.304 | 0.050 |

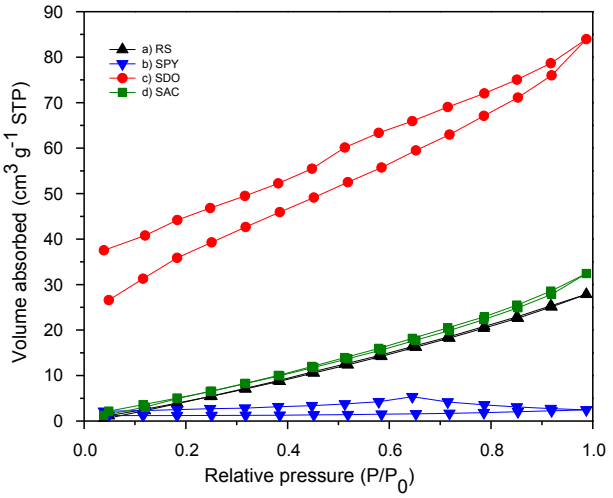


**Fig. 3 – Nitrogen adsorption/desorption isotherms of a) raw *Sargassum* spp. (RS), b) pyrolyzed (SPY), c) doped (SDO) and d) activated (SAC).**

Please cite this article in press as: Escobar B, et al., N-doped porous carbon from *Sargassum* spp. as metal-free electrocatalysts for oxygen reduction reaction in alkaline media, International Journal of Hydrogen Energy (2017), http://dx.doi.org/10.1016/j.ijhydene.2017.06.240

### XPS-analysis

XPS analysis was performed to evaluate the chemical bonding states and elemental composition of the biocarbons surface after the doping and activation processes. XPS survey is summarized in Table 3. Carbon is the element that is in greater concentration in the all samples surface (>65% at.), followed by oxygen (>20% at.), while nitrogen is about 1.5–1.8% at. It can also be seen that RS and SYP samples have calcium because this is characteristics in the source of seaweed.

High-resolution spectra provide more information about the N–C bonding configuration. The N 1s spectra are shown in Fig. 3 and could be deconvoluted in two peaks with binding energies of 398.2–398.5 eV and 400.1–400.7 eV which correspond to N-pyridinic and N-pyrrolic nitrogen-carbon bonds, respectively [30]. This can be represented as nitrogen atoms bound to the edges of graphite layers [31]. It is interesting to notice that the pyrolyzed seaweed is the only one which presents N-oxides pyridinic bond which plays an important role in the ORR process [30].

As it is observed in Table 3, the relative % at. of the N-pyridinic change from RS sample to SAC sample, decreasing from 46.4% at. to 38.2% at. While this atomic concentration remains similar in RS sample (46.4% at.) and SDO (45% at.). It has been reported that N-pyridinic and N-graphitic nitrogen play the most important role in the ORR performance of graphene-derived materials [32].

### Elemental analysis

Additionally, elemental analysis was performed to determinate the chemical composition in the bulk of the N-doped carbons. Usually, carbons derived from biomass are rich in nitrogen and oxygen functional groups [33]. The biocarbons synthesized in this work have a low load of nitrogen (less than 1%wt) and sulfur (0.22–1.05 %wt) in the bulk, the elemental analysis results are shown in Table 4. An average of C/H/N/S analysis values revealed that the nitrogen content in RS is relatively low (0.94 %wt ± 0.21), in comparison with others seaweeds species. Besides, *Sargassum* spp. has a carbon content around 35.90%wt. During biomass pyrolysis, nitrogen is release forming NH3 and HCN from NOx precursors [34]; for this reason in SYP sample decrease the nitrogen content (0.56 %wt ± 0.31). However, it is noteworthy that the sulfur content increases almost double, this may be because the sulfur compounds are heavier than the nitrogen compounds and therefore not released as easy, remaining in higher concentration after the pyrolysis. On the other hand, with the doping process the nitrogen content increases from 0.56 to 0.92%wt. This result demonstrates that doping treatment proposed in this work is effective to incorporate nitrogen species into carbonaceous materials. However, solvothermal treatment remove sulfur species. Finally, SAC sample has nitrogen content very close to 0.95 %wt. This results indicate that a certain amount of carbon attacked by alkali was removed increasing the nitrogen concentration. A certain amount of sulfur is removed during activation treatment too.

**Table 4 – CHNS elemental analyses of the bulk of RS and N-doped carbons from *Sargassum* spp.**

| Sample | N (wt%) | C (wt%) | H (wt%) | S (wt%) |
|---|---|---|---|---|
| RS | 0.94 ± 0.21 | 35.90 ± 5.23 | 4.85 ± 0.16 | 0.58 ± 0.50 |
| SPY | 0.56 ± 0.31 | 36.63 ± 1.34 | 0.68 ± 0.08 | 1.05 ± 0.23 |
| SDO | 0.92 ± 0.07 | 45.69 ± 0.32 | 0.94 ± 0.06 | 0.25 ± 0.16 |
| SAC | 0.95 ± 0.02 | 14.39 ± 0.24 | 1.58 ± 0.35 | 0.22 ± 0.07 |

### Fourier transform infrared spectroscopy

Fig. 4 shows the FT-IR spectra of metal-free electrocatalysts from *Sargassum* spp. prepared by different methods. The FTIR spectra showed different peaks, which confirmed the presence of functional groups such as hydroxyl, amine, methyl, carboxylic, etc.

RS has hydroxyl stretch (–OH) or amine groups (N–H) in the region of 3700 to 3000 $cm^{-1}$ [35], this band is broad due to the presence of a large density of hydrogen bonds, mainly hydroxyl radicals in the polysaccharide pyranose rings [36]. The bands at 2921 to 2346 $cm^{-1}$ are assigned to C–H stretching vibrations ($-CH_3$ and $CH_2$ groups) [37]. The weaker symmetrical band at 1602 $cm^{-1}$ corresponds to the asymmetrical stretching of the carbonyl double bond from the carboxylic functional group (C=O) [38], and the band at 1424 $cm^{-1}$ is originated from the bending vibrations of O–H bond [39]. The bands around 1056 $cm^{-1}$are due to –C–O stretching of alcoholic groups. The region between 1250 and 1000 $cm^{-1}$ shows bands mainly attributed to oxygenated groups (C–O bonds) in alcohols, ethers, and carboxylic acids [8], while between 1000 and 400 $cm^{-1}$correspond to sugar vibrations [36].

SPY and SDO samples have an intense peak around 1409 $cm^{-1}$, which may be due to the increased formation of group hydroxyl and carbonyl (C=O). A new peak appears around 2160 $cm^{-1}$ related to the thiocyanate group concerning to sulfur in the seaweeds and registered in CHONS analysis, while the peak at 2363 $cm^{-1}$ could be the –CH stretch and $H_3O^+$ [26]. Pyrolysis treatment modifies considerably the

**Table 3 – Surface chemical composition determinate by XPS and the relative composition of N–C bonds.**

| Samples | Elemental composition (% at.) | | | | | Chemical states of N with their relative concentration (%) and their B.E (eV) | | |
|---|---|---|---|---|---|---|---|---|
| | C | O | N | Ca | S | N pyridinic | N pyrrolic | N4-pyridinic-N-oxide |
| RS | 74.6 | 20.3 | 1.5 | 3.6 | | 46.4 (398.4) | 53.6 (400.1) | |
| SPY | 65.6 | 23.5 | 1.8 | 7.5 | 1.8 | 33.5 (398.2) | 45.7 (400.4) | 20.8 (402.6) |
| SDO | 70.1 | 28.1 | 1.8 | | | 45 (398.5) | 55 (400.5) | |
| SAC | 67.7 | 30.5 | 1.8 | | | 38.2 (398.4) | 61.8 (400.7) | |

Please cite this article in press as: Escobar B, et al., N-doped porous carbon from *Sargassum* spp. as metal-free electrocatalysts for oxygen reduction reaction in alkaline media, International Journal of Hydrogen Energy (2017), http://dx.doi.org/10.1016/j.ijhydene.2017.06.240

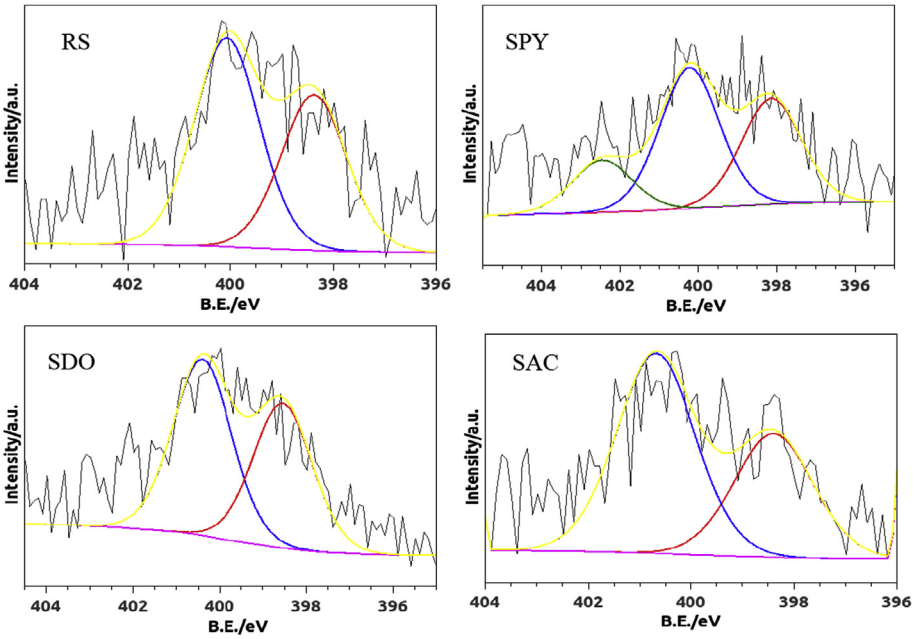


**Fig. 4 – High-resolution XPS spectra in the N1s region of RS, SPY, SDO and SAC samples.**

functional groups that compose N-doped carbons compared to the raw material. The SAC sample shows a broad band that appeared at 3200 $cm^{-1}$, this band is attributed to the overlapping of the O–H and N–H stretching vibration [40]. The peak at 1409 cm-1 is assigned to O–H and C=O bending vibration. The principal absorption bands and their respective reactive group are listed in Table 5, which are typically found in the seaweeds.

### *Raman spectroscopy*

Raman spectrum shown in Fig. 5 was performed between 500 and 3500 $cm^{-1}$, where is observed two strong peaks at ~1569 $cm^{-1}$ (G-band) and ~1326 $cm^{-1}$ (D-band) for all N-doped carbons, as expected for partially graphitized carbons [41]. The D-band is associated with a double-resonance Raman process in highly disordered carbons. In this study, the $I_D/I_G$ ratio was calculated and used as indicator of the disorder degree (edges and/or defects) in the carbon lattice of the N-doped carbons. A ratio $I_D/I_G = 0$ corresponds to perfect graphitic lattice. RS sample has an $I_D/I_G$ ratio of 1.79 ± 0.08 indicating the presence of high disorder in the carbon amorphous raw material. After pyrolysis, $I_D/I_G$ ratio decreased to 1.43 ± 0.02 for SPY sample, which indicates that graphitic carbon is formed during the pyrolysis. SDO sample has an $I_D/I_G$ ratio of 1.35 ± 0.01, this sample has the higher graphitic degree and less disordered structure, which was promoted by the solvothermal treatment. Finally, SAC sample has a $I_D/I_G$ ratio of 1.61 ± 0.05, which indicates that activation treatment cause damage in the graphitic structure of the pyrolyzed carbon [42]. All results obtained indicated a high disorder in the carbon structure of samples.

**Table 5 – FT-IR absorption frequencies ($cm^{-1}$) and their relation with the functional groups found for the RS and N-doped carbons from *Sargassum* spp.**

| Sample | Wavenumber ($cm^{-1}$) | Bond | Group |
|---|---|---|---|
| RS | 3700–3000 | O–H, N–H | Hydroxyl, amine |
| | 2921 | C–H | Methyl |
| | 2346 | C–H | Methyl |
| | 1602 | C=O | Carboxylic |
| | 1427 | O–H | Hydroxyl |
| | 1056 | C–O | Carbonyl |
| | 1029 | C–O, C–N | Carbonyl, C–N stretching |
| | 854 | C–N, N–H | C–N stretching, amine |
| SPY | 2363 | C–H | Methyl |
| SDO | 2160 | S–C≡N | Thiocyanate |
| | 1409 | O–H, C=O | Hydroxyl, carboxyl |
| | 871 | C=O | Carboxyl |
| | 711 | C=O | $CO_2$ |
| SAC | 3200 | O–H, N–H | Hydroxyl, amine |
| | 1409 | O–H, C=O | Hydroxyl, carboxyl |

Please cite this article in press as: Escobar B, et al., N-doped porous carbon from *Sargassum* spp. as metal-free electrocatalysts for oxygen reduction reaction in alkaline media, International Journal of Hydrogen Energy (2017), http://dx.doi.org/10.1016/j.ijhydene.2017.06.240

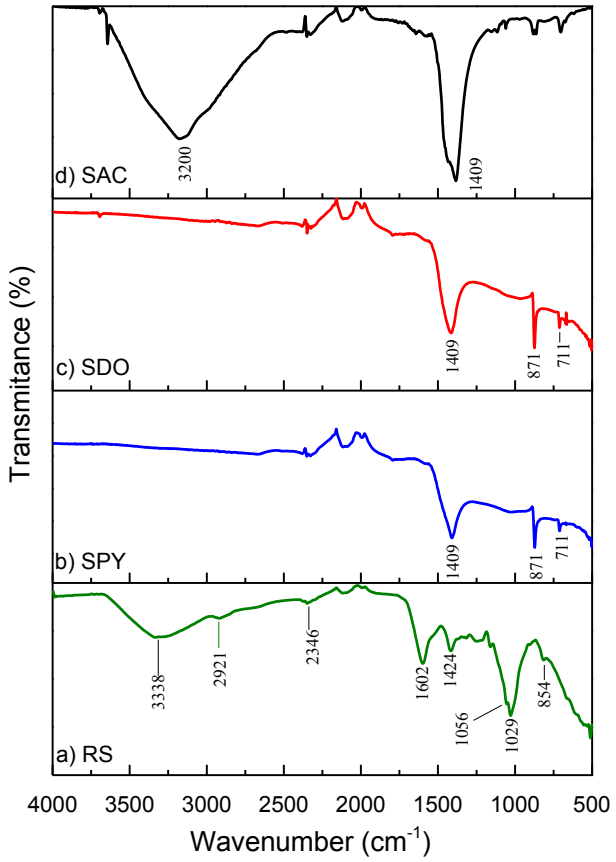


**Fig. 5 – FT-IR spectra of samples a) RS, b) SPY, c) SDO and d) SAC.**

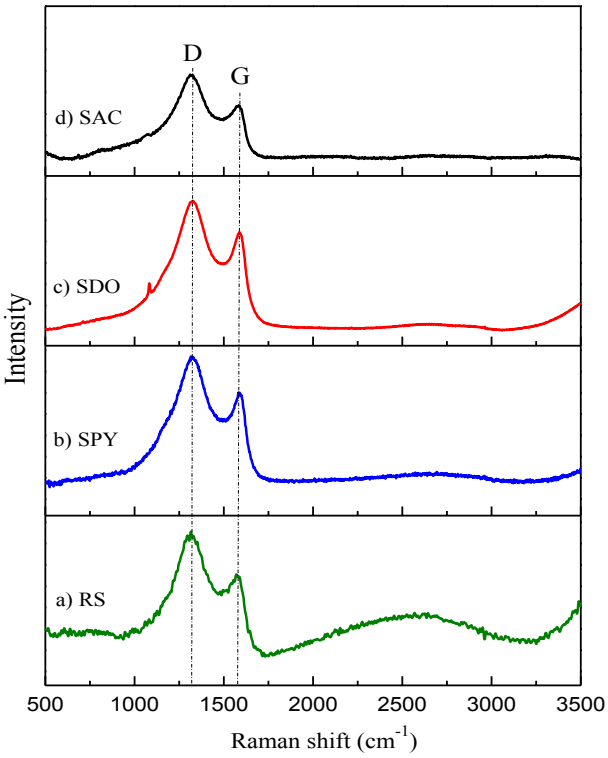


**Fig. 6 – Raman spectroscopy of samples a) raw *Sargassum* spp. (RS), b) pyrolyzed (SPY), c) doped (SDO) and d) activated (SAC).**

### *Electrochemical characterization*

Fig. 6 shows cyclic voltammograms (CV) of SAC, SDO and SPY recorded at window potential from 0 to 1.2 V vs RHE electrode, at a scan rate of 20 $mVs^{-1}$ in 0.5 M KOH electrolyte saturated with $N_2$. The three metal-free electrocatalysts from *Sargassum* spp. show the regular pseudo-capacitive behavior [43]. There are not redox reactions peaks typically attributed to supercapacitive behavior [44]. SPY sample shows the lowest current density, which is to be expected due to its low $S_{BET}$. However, SDO shows higher current density than SPY but lower than SAC, this can be attributed to acid wash during the activation process, which according to previous studies enhances the electrocatalyst performance by 2 or 6 times after acid leaching [19]. Also, the increase in the current density for both SDO and SAC samples is in accordance with the increase in N content obtained by CHNS analysis. In addition, SAC sample has highest current density, this is attributed to the functional groups on its surface. Furthermore, this sample has the highest heteroatoms content ratio as shown in Table 4 [45].

ORR performance was evaluated by linear sweep voltammetry (LSV) using rotating disk electrode (RDE) technique in O2-saturated electrolyte solution of 0.5 M KOH. The ORR polarization curves obtained for SAC, SDO and SPY are shown in Fig. 7, which were performed at a potential scan rate of 5 mV $s^{-1}$ under different electrode rotation rates (200, 400, 800, 1200, 1600 and 2000 rpm). The three metal-free electrocatalyst shows activity for the ORR, and as to be expected, the current density increase with the speed rotation rate increase (Fig. 8a–c). Fig. 7d show the comparison of the ORR performance of the three metal-free electrocatalyst from *Sargassum* spp. and a commercial electrocatalyst based Pt (20 wt% Pt/Vulcan, BASF), while Table 6 summarized the electrochemical parameters obtained from Fig. 8. SPY has the lowest current

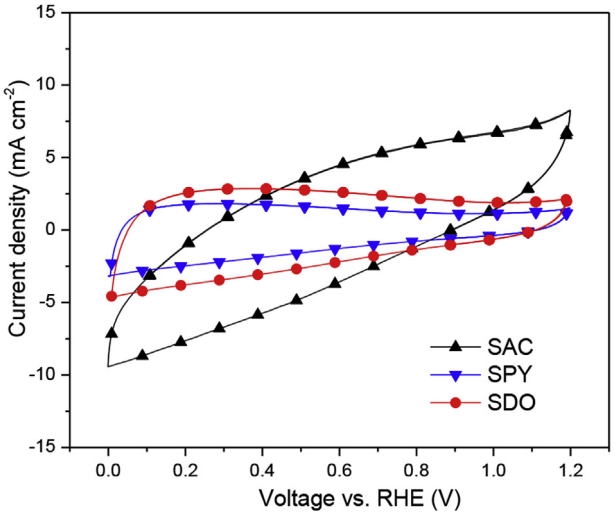


**Fig. 7 – Cyclic voltammetry of SPY, SDO and SAC, in alkaline electrolyte saturated with $N_2$ at scan rate of 20 $mVs^{-1}$.**

Please cite this article in press as: Escobar B, et al., N-doped porous carbon from *Sargassum* spp. as metal-free electrocatalysts for oxygen reduction reaction in alkaline media, International Journal of Hydrogen Energy (2017), http://dx.doi.org/10.1016/j.ijhydene.2017.06.240

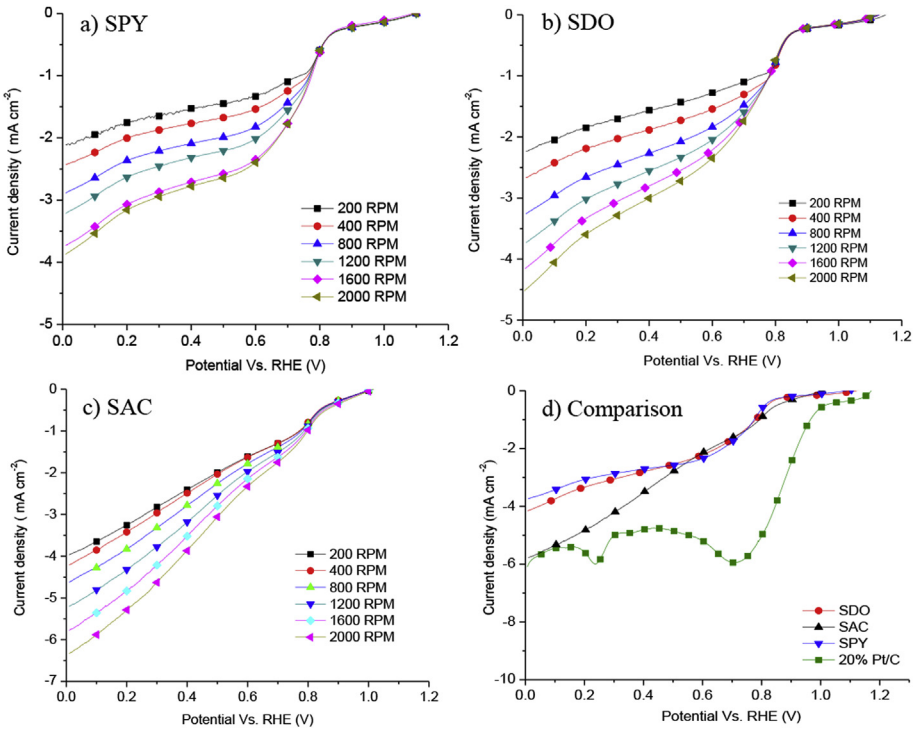


**Fig. 8 – LSV curves for a) SPY, b) SDO, c) SAC and d) LSV of three N-doped carbons compared with commercial 20 wt% Pt/C catalysts at 1600 rpm. The measures were performed in $O_2$-saturated 0.5 M KOH solution at scan rates of 5 mV $s^{-1}$.**

density at 0.2 V vs. RHE (3.1 mA $cm^{-2}$). Moreover, SDO had a slightly higher current density than SYP at 0.2 V vs. RHE (3.3 mA $cm^{-2}$), may be due to this metal-free electrocatalyst has highest SBET and major content of N incorporated into the carbon lattice than SYP. On the other hand, SAC show the highest current density of the three metal-free electrocatalyst (4.78 mA $cm^{-2}$ at 0.2 V vs. RHE). This can be attributed to the increase in the SBET respect to SYP, and the functional groups on the SAC metal-free electrocatalyst surface. This agrees with previous studies that confirm that electrocatalytic activity depends more of the surface chemistry than of the SBET value. The ORR performance for commercial 20 wt% Pt/Vulcan was also graphed for comparison purposes. SAC shows the highest current density very close to Pt/Vulcan electrocatalyst (5.6 mA $cm^{-2}$ at 0.2 V vs. RHE) and an onset potential of 0.838 V. Fig. 8d). Additionally, SDO sample has the highest onset potential (0.852 V vs. RHE) among three metal-free electrocatalyst. The onset potential and current density values evaluated in this work are comparable with the values reported in recent studies for N-doped carbon derived from other biomass sources [46–48].

**Table 6 – Electrocatalytic parameters of the ORR performance of SPY, SDO, SAC and 20 wt% Pt/C.**

| Sample | On-set potential (V vs. RHE) | Current density at 0.2 V (mA $cm^{-2}$) |
|---|---|---|
| SPY | 0.826 | 3.1 |
| SAC | 0.838 | 4.8 |
| SDO | 0.852 | 3.3 |
| 20 wt% Pt/C | 1.000 | 5.6 |

The chemical composition of the electrocatalyst surface and N–C type of bond is very important for the ORR. These metal-free electrocatalysts show high activity for the ORR, especially SAC sample. SYP and SDO has a very similar performance for the ORR. Although, the three metal-free electrocatalysts have the same concentration of N in their surface, the configuration of N–C bonds change according to the chemical treatment. Borghei et al. (2017) reported that doping treatment significantly affected the activity for the ORR because provide more functional groups on the surface of carbon increasing the N-doping loading [53]. This working group synthetized biocarbons from coconut shells doped with urea as nitrogen precursor, the activity for ORR was evaluated in alkaline media and is comparable with the results reported in this work. Furthermore, it has been reported that the limit current density for ORR is promoted by the N-graphitic bond, while the N-pyridinic bonds improves the onset potential [49]. SDO sample has the better onset potential value (0.852 V vs. RHE) may because this metal-free electrocatalyst has the highest concentration of N-pyridinic bonds. Moreover, SYP and SAC samples has a very similar concentration of N-pyridinic bonds, and their onset potential value is similar too. An alternative to improve the performance of these promising metal-free electrocatalysts would be to motif the synthesis conditions, in order to promote the formation of more N-pyridinic and N-quaternary groups on the biocarbons surface. This could be achieved by pyrolyzing at higher temperatures.

Please cite this article in press as: Escobar B, et al., N-doped porous carbon from *Sargassum* spp. as metal-free electrocatalysts for oxygen reduction reaction in alkaline media, International Journal of Hydrogen Energy (2017), http://dx.doi.org/10.1016/j.ijhydene.2017.06.240

## Conclusions

*Sargassum* spp. is abundant and renewable source of carbon and other heteroatoms. Therefore, in this work it was evaluated as raw material for the synthesis of N-doped carbons as metal-free electrocatalyst for alkaline fuel cells. Three electrocatalyst wit promising properties were obtained by pyrolysis (SYP), doped (SDO) and activation (SAC) treatments. TGA show high yield for the pyrolysis at 700 °C. of *Sargassum* spp. (≈40%wt). Carbonization of raw material was confirmed by Raman spectroscopy. After doping treatment, SDO sample shows an increase in $S_{BET}$ from 3.864 $m^2\ g^{-1}$ to 133.871 $m^2\ g^{-1}$ and high activity for ORR with the highest onset potential (0.852 V) among three samples. Besides, SAC sample exhibited the highest current density at 0.2 V vs. RHE (4.78 mA $cm^{-2}$) and an onset potential of 0.838 V. Furthermore, *Sargassum* spp. inundations is an actual problem for the tourist industry, thereby using it as raw material to obtain metal-free electrocatalyst with high performance for ORR, could be a promising alternative to solve one of the biggest challenges in fuel cells.

## Acknowledgements

The authors would like to thank to LANNBIO Cinvestav-Mérida for the XPS measurements, under financial support of FOMIX-Yucatán 2008-108160, CONACYT LAB-2009-01 (No. 123913) and CB-2015-250632, Infraestructura 2015-253986 and LENERSE-254667 grants. Also, the authors appreciate the technical support of Msc. D Huerta, Eng. W. Cauich and Msc. Martín Baas.

## REFERENCES

[1] Yu Y, Wang C, Guo X, Paul Chen J. Modification of carbon derived from *Sargassum* sp. by lanthanum for enhanced adsorption of fluoride. J Colloid Interface Sci 2015;441:113–20. http://dx.doi.org/10.1016/j.jcis.2014.10.039.

[2] Schell BJM, Goodwin DS, Siuda ANS. Recent *Sargassum* inundation events in the caribbean: shipboard observations reveal dominance of a previously rare form. Oceanography 2015;28:8–10. http://dx.doi.org/10.5670/oceanog.2015.70.

[3] Wang M, Hu C. Mapping and quantifying *Sargassum* distribution and coverage in the Central West Atlantic using MODIS observations. Remote Sens Environ 2016;183:350–67. http://dx.doi.org/10.1016/j.rse.2016.04.019.

[4] Lourenço SO, Barbarino E, De-Paula JC, Pereira LODS, Lanfer Marquez UM. Amino acid composition, protein content and calculation of nitrogen-to-protein conversion factors for 19 tropical seaweeds. Phycol Res 2002;50:233–41. http://dx.doi.org/10.1046/j.1440-1835.2002.00278.x.

[5] Stratford JP, Hutchings TR, de Leij FAAM. Intrinsic activation: the relationship between biomass inorganic content and porosity formation during pyrolysis. Bioresour Technol 2014;159:104–11. http://dx.doi.org/10.1016/j.biortech.2014.02.064.

[6] Li R, Wei Z, Gou X. Nitrogen and phosphorus dual-doped graphene/carbon nanosheets as bifunctional electrocatalysts for oxygen reduction and evolution. ACS Catal 2015;5:4133–42. http://dx.doi.org/10.1021/acscatal.5b00601.

[7] Sun T, Xu L, Li S, Chai W, Huang Y, Yan Y, et al. Cobalt-nitrogen-doped ordered macro-/mesoporous carbon for highly efficient oxygen reduction reaction. Appl Catal B Environ 2016;193:1–8. http://dx.doi.org/10.1016/j.apcatb.2016.04.006.

[8] Li W, Tan S, Shi Y, Li S. Utilization of *sargassum* based activated carbon as a potential waste derived catalyst for low temperature selective catalytic reduction of nitric oxides. Fuel 2015;160:35–42. http://dx.doi.org/10.1016/j.fuel.2015.07.045.

[9] Zhang Z, Wan M, Wei Y. Highly crystalline polyaniline nanostructures doped with dicarboxylic acids. Adv Funct Mater 2006;16:1100–4. http://dx.doi.org/10.1002/adfm.200500636.

[10] Borghei M, Laocharoen N, Kibena-Põldsepp E, Johansson LS, Campbell J, Kauppinen E, et al. Porous N,P-doped carbon from coconut shells with high electrocatalytic activity for oxygen reduction: alternative to Pt-C for alkaline fuel cells. Appl Catal B Environ 2017;204:394–402. http://dx.doi.org/10.1016/j.apcatb.2016.11.029.

[11] Choi CH, Park SH, Woo SI. Heteroatom doped carbons prepared by the pyrolysis of bio-derived amino acids as highly active catalysts for oxygen electro-reduction reactions. Green Chem 2011;13:406–12. http://dx.doi.org/10.1039/C0GC00384K.

[12] Zhao J, Liu Y, Quan X, Chen S, Yu H, Zhao H. Nitrogen-doped carbon with a high degree of graphitization derived from biomass as high-performance electrocatalyst for oxygen reduction reaction. Appl Surf Sci 2017;396:986–93. http://dx.doi.org/10.1016/j.apsusc.2016.11.073.

[13] Paraknowitsch JP, Thomas A. Doping carbons beyond nitrogen: an overview of advanced heteroatom doped carbons with boron, sulphur and phosphorus for energy applications. Energy Environ Sci 2013;6:2839. http://dx.doi.org/10.1039/c3ee41444b.

[14] Fang Y, Wang H, Yu H, Peng F. From chicken feather to nitrogen and sulfur co-doped large surface bio-carbon flocs : an ef fi cient electrocatalyst for oxygen reduction reaction. Electrochim Acta 2016;213:273–82. http://dx.doi.org/10.1016/j.electacta.2016.07.121.

[15] Chouler J, Padgett GA, Cameron PJ, Preuss K, Titirici MM, Ieropoulos I, et al. Towards effective small scale microbial fuel cells for energy generation from urine. Electrochim Acta 2016;192:89–98. http://dx.doi.org/10.1016/j.electacta.2016.01.112.

[16] Zheng X, Cao X, Wu J, Tian J, Jin C, Yang R. Yolk-shell N/P/B ternary-doped biocarbon derived from yeast cells for enhanced oxygen reduction reaction. Carbon NY 2016;107:907–16. http://dx.doi.org/10.1016/j.carbon.2016.06.102.

[17] Elmouwahidi A, Vivo-Vilches JF, Pérez-Cadenas AF, Maldonado-Hódar FJ, Carrasco-Marín F. Free metal oxygen-reduction electro-catalysts obtained from biomass residue of the olive oil industry. Chem Eng J 2016;306:1109–15. http://dx.doi.org/10.1016/j.cej.2016.08.042.

[18] Liu Y, Ruan J, Sang S, Zhou Z, Wu Q. Iron and nitrogen co-doped carbon derived from soybeans as efficient electro-catalysts for the oxygen reduction reaction. Electrochim Acta 2016;215:388–97. http://dx.doi.org/10.1016/j.electacta.2016.08.090.

[19] Liu F, Peng H, Qiao X, Fu Z, Huang P, Liao S. High-performance doped carbon electrocatalyst derived from soybean biomass and promoted by zinc chloride. Int J Hydrogen Energy 2014;39:10128–34. http://dx.doi.org/10.1016/j.ijhydene.2014.04.176.

[20] Wang R, Wang H, Zhou T, Key J, Ma Y, Zhang Z, et al. The enhanced electrocatalytic activity of okara-derived N-doped mesoporous carbon for oxygen reduction reaction. J Power

Sources 2015;274:741–7. http://dx.doi.org/10.1016/j.jpowsour.2014.10.049.
[21] Huang H, Wei X, Gao S. Nitrogen-doped porous carbon derived from Malachium aquaticum biomass as a highly efficient electrocatalyst for oxygen reduction reaction. Electrochim Acta 2016;220:427–35. http://dx.doi.org/10.1016/j.electacta.2016.10.108.
[22] Alatalo S-M, Qiu K, Preuss K, Marinovic A, Sevilla M, Sillanpää M, et al. Soy protein directed hydrothermal synthesis of porous carbon aerogels for electrocatalytic oxygen reduction. Carbon NY 2016;96:622–30. http://dx.doi.org/10.1016/j.carbon.2015.09.108.
[23] Dhelipan M, Arunchander A, Sahu AK, Kalpana D. Activated carbon from orange peels as supercapacitor electrode and catalyst support for oxygen reduction reaction in proton exchange membrane fuel cell. J Saudi Chem Soc 2016. http://dx.doi.org/10.1016/j.jscs.2016.12.003.
[24] Lardizabal-Guitierrez D, González-Quijano D, Bartolo-Pérez P, Escobar-Morales B, Rodríguez-Varela FJ, Alonso-Lemus IL. Communication—synthesis of self-doped metal-free electrocatalysts from waste leather with high ORR activity. J Electrochem Soc 2016;163:H15–7. http://dx.doi.org/10.1149/2.0191602jes.
[25] Wang S, Wang Q, Hu YM, Xu SN, He ZX, Ji HS. Study on the synergistic co-pyrolysis behaviors of mixed rice husk and two types of seaweed by a combined TG-FTIR technique. J Anal Appl Pyrol 2015;114:109–18. http://dx.doi.org/10.1016/j.jaap.2015.05.008.
[26] Ceylan S, Goldfarb JL. Green tide to green fuels: TG-FTIR analysis and kinetic study of Ulva prolifera pyrolysis. Energy Convers Manag 2015;101:263–70. http://dx.doi.org/10.1016/j.enconman.2015.05.029.
[27] López-González D, Fernandez-Lopez M, Valverde JL, Sanchez-Silva L. Pyrolysis of three different types of microalgae: kinetic and evolved gas analysis. Energy 2014;73:33–43. http://dx.doi.org/10.1016/j.energy.2014.05.008.
[28] Tag AT, Duman G, Ucar S, Yanik J. Effects of feedstock type and pyrolysis temperature on potential applications of biochar. J Anal Appl Pyrol 2016;120:200–6. http://dx.doi.org/10.1016/j.jaap.2016.05.006.
[29] Song W, Guo M. Quality variations of poultry litter biochar generated at different pyrolysis temperatures. J Anal Appl Pyrol 2012;94:138–45. http://dx.doi.org/10.1016/j.jaap.2011.11.018.
[30] Daems N, Sheng X, Vankelecom IFJ, Pescarmona PP. Metal-free doped carbon materials as electrocatalysts for the oxygen reduction reaction. J Mater Chem A 2014;2:4085. http://dx.doi.org/10.1039/c3ta14043a.
[31] Sahraie NR, Paraknowitsch JP, Go C, Thomas A, Strasser P. Noble-metal-free electrocatalysts with enhanced ORR performance by task-specific functionalization of carbon using ionic liquid precursor systems. 2014.
[32] Kim H, Lee K, Woo SI, Jung Y. On the mechanism of enhanced oxygen reduction reaction in nitrogen-doped graphene nanoribbons. Phys Chem Chem Phys 2011;13:17505. http://dx.doi.org/10.1039/c1cp21665a.
[33] Elmouwahidi A, Zapata-Benabithe Z, Carrasco-Marín F, Moreno-Castilla C. Activated carbons from KOH-activation of argan (Argania spinosa) seed shells as supercapacitor electrodes. Bioresour Technol 2012;111:185–90. http://dx.doi.org/10.1016/j.biortech.2012.02.010.
[34] Becidan M, Skreiberg Ø, Hustad JE. NOx and $N_2O$ precursors ($NH_3$ and HCN) in pyrolysis of biomass residues. Energy Fuels 2007;21:1173–80. http://dx.doi.org/10.1021/ef060426k.
[35] Deng L, Su Y, Su H, Wang X, Zhu X. Sorption and desorption of lead (II) from wastewater by green algae Cladophora fascicularis. J Hazard Mater 2007;143:220–5. http://dx.doi.org/10.1016/j.jhazmat.2006.09.009.
[36] Oliveira RC, Hammer P, Guibal E, Taulemesse JM, Garcia O. Characterization of metal-biomass interactions in the lanthanum(III) biosorption on *Sargassum* sp. using SEM/EDX, FTIR, and XPS: preliminary studies. Chem Eng J 2014;239:381–91. http://dx.doi.org/10.1016/j.cej.2013.11.042.
[37] Chen Y, Mao W, Gao Y, Teng X, Zhu W, Chen Y, et al. Structural elucidation of an extracellular polysaccharide produced by the marine fungus Aspergillus versicolor. Carbohydr Polym 2013;93:478–83. http://dx.doi.org/10.1016/j.carbpol.2012.12.047.
[38] Hackbarth FV, Girardi F, de Souza SMAGU, de Souza AAU, Boaventura RAR, Vilar VJP. Marine macroalgae Pelvetia canaliculata (Phaeophyceae) as a natural cation exchanger for cadmium and lead ions separation in aqueous solutions. Chem Eng J 2013;242:294–305. http://dx.doi.org/10.1016/j.cej.2013.12.043.
[39] Shao P, Chen X, Sun P. Chemical characterization, antioxidant and antitumor activity of sulfated polysaccharide from *Sargassum horneri*. Carbohydr Polym 2014;105:260–9. http://dx.doi.org/10.1016/j.carbpol.2014.01.073.
[40] Altintig E, Arabaci G, Altundag H. Preparation and characterization of the antibacterial efficiency of silver loaded activated carbon from corncobs. Surf Coatings Technol 2016;304:63–7. http://dx.doi.org/10.1016/j.surfcoat.2016.06.077.
[41] Pérez-Villar S, Lanz P, Schneider H, Novák P. Characterization of a model solid electrolyte interphase/carbon interface by combined in situ Raman/Fourier transform infrared microscopy. Electrochim Acta 2013;106:506–15. http://dx.doi.org/10.1016/j.electacta.2013.05.124.
[42] Song LT, Wu ZY, Liang HW, Zhou F, Yu ZY, Xu L, et al. Macroscopic-scale synthesis of nitrogen-doped carbon nanofiber aerogels by template-directed hydrothermal carbonization of nitrogen-containing carbohydrates. Nano Energy 2016;19:117–27. http://dx.doi.org/10.1016/j.nanoen.2015.10.004.
[43] Zhou L, Fu P, Wen D, Yuan Y, Zhou S. Self-constructed carbon nanoparticles-coated porous biocarbon from plant moss as advanced oxygen reduction catalysts. Appl Catal B Environ 2016;181:635–43. http://dx.doi.org/10.1016/j.apcatb.2015.08.035.
[44] Yan W, Yu WJ, Wang L, Zhang D, Ge XQ, Hang JZ, et al. Preparation of partially reduced graphene oxide nanosheets/poly(sodium 4-styrenesulfonate) composite with high capacitance. Electrochim Acta 2014;147:257–64. http://dx.doi.org/10.1016/j.electacta.2014.09.120.
[45] Wang D, Geng Z, Li B, Zhang C. High performance electrode materials for electric double-layer capacitors based on biomass-derived activated carbons. Electrochim Acta 2015;173:377–84. http://dx.doi.org/10.1016/j.electacta.2015.05.080.
[46] Han C, Wang S, Wang J, Li M, Deng J, Li H, et al. Controlled synthesis of sustainable N-doped hollow core-mesoporous shell carbonaceous nanospheres from biomass. Nano Res 2014;7:1809–19. http://dx.doi.org/10.1007/s12274-014-0540-x.
[47] Alonso-Lemus IL, Rodriguez-Varela FJ, Figueroa-Torres MZ, Sanchez-Castro ME, Hernandez-Ramírez A, Lardizabal-Gutierrez D, et al. Novel self-nitrogen-doped porous carbon from waste leather as highly active metal-free electrocatalyst for the ORR. Int J Hydrogen Energy 2016;1:4–11. http://dx.doi.org/10.1016/j.ijhydene.2016.09.033.
[48] Guo C, Li Z, Niu L, Liao W, Sun L, Wen B, et al. A nanopore-structured nitrogen-doped biocarbon electrocatalyst for oxygen reduction from two-step carbonization of lemna minor biomass. Nanoscale Res Lett 2016;11:268. http://dx.doi.org/10.1186/s11671-016-1489-3.
[49] Dai L, Xue Y, Qu L, Choi HJ, Baek JB. Metal-free catalysts for oxygen reduction reaction. Chem Rev 2015;115:4823–92. http://dx.doi.org/10.1021/cr5003563.

Please cite this article in press as: Escobar B, et al., N-doped porous carbon from *Sargassum* spp. as metal-free electrocatalysts for oxygen reduction reaction in alkaline media, International Journal of Hydrogen Energy (2017), http://dx.doi.org/10.1016/j.ijhydene.2017.06.240